Improvement of Polar Snow Microwave Brightness Temperature Simulations for Dense Wind Slab and Large Grain

Julien Meloche, Alain Royer, Alexandre Roy, *Member, IEEE*, Alexandre Langlois, and Ghislain Picard

Abstract— The Arctic snowpack, characterized mainly by a dense wind slab (WS) layer overlaying less dense and porous depth hoar (DH), generates large uncertainties in microwave radiative transfer models (RTM) used to interpret satellite observations. In this work, we tested two improvements recently implemented in the snow microwave radiative transfer (SMRT) model. First, an improvement of the snow microstructure parametrizations introduces a polydispersity geometrical parameter (K) related to the grain shape and microstructural arrangement. Second, the new electromagnetic model (EM) based on the strong contrast expansion (SCE) allows a continuous formulation of the scattering coefficient as a function of the density between low-density snow and hard and icy snow. The SCE model was compared with in situ observations to the commonly used improve Born approximation (IBA) EM. Results show improved brightness temperature simulations at 19, 37, and 89 GHz compared to surface-based and satellite microwave radiometric measurements using polydispersity values ($K_{WS} = 0.80$ and $K_{DH} = 1.33$) for scaling the measured optical grain size of the different snow layers with IBA. The finding is that the polydispersity values found in this study are of general applicability for Polar-layered snowpack. The SCE model yields results similar to IBA for snow densities up to 500 kg m^{-3} but no analysis was investigated for the range of 500–700 kg m^{-3} (firn). These improvements in snow microstructure and the new SCE RTM allow better simulations of Polar snow and therefore better Polar snowpack monitoring by satellite.

Index Terms— Arctic snow, microwave grain size, polydispersity, snow microwave radiative transfer (SMRT) model.

I. INTRODUCTION

MICROWAVE radiometry of snow shows great potential; it has been widely used to collect information on the snowpack, allowing the understanding of energy and mass exchange processes between the snowpack and the atmosphere, which significantly impact the global climate and water resources [34], [38]. Improving retrieval of snow properties such as snow water equivalent (SWE) from microwave satellite observations is gaining traction with future satellite missions [5], [7], [18]. However, enhanced microwave radiative transfer modeling simulating satellite observations is needed. Modeling of snowpack microwave emission has to be improved because of the complex physical properties of snow (microstructure, stratigraphy) owing to metamorphism processes [1], [21], [30], [32]. This affects the radiative transfer of microwave radiation through the snowpack [16]. The problem is particularly challenging for Arctic snow, which is characterized by two layers with very different characteristics: a dense surface layer deposited and scoured by the wind [wind slab (WS)], and a basal layer composed of large metamorphized crystals of ice depth hoar (DH) [20], [29], [33], [36]. Indeed, wind-induced snow drifting leads to the sublimation of snow crystals and their compaction into hard WSs with densities up to 400–600 kg m^{-3} near the surface. This very hard snow surface at the transition between snow and icy snow is still poorly resolved in microwave radiative transfer models (RTM).

Conversely, at the bottom of the snowpack, snow evolves toward large hoar crystals due to the strong vertical thermal gradient within the snowpack. DH crystals can reach up to a few centimeters and feature various shapes (cup-shaped, hollow or striated skeleton-type crystals arranged in prisms, and chains or glassy faces) and reduced bond strengths between ice crystals [9]. This leads to a DH layer with high heterogeneity in microstructural shape and size which is not well captured in current representations of microwave scattering.

The contrasted stratification of the Arctic snowpack in two main layers (WS and DH) strongly contributes to modify the microwave emission compared to lower latitudes. In general, scattering significantly increases with snow density, grain size, and grain aggregation (stickiness) (see [22], [25]). Commonly used RTMs often fail with such extreme characteristics of the Arctic snowpack [12], [28], [32], [36], [38], which differ from the usual snow conditions of temperate or boreal environments. This article aims to address these two problems of microstructure and high density specific to Arctic snow.

Recent progress has been made to simulate microwave radiation propagation through the snowpack in the snow microwave radiative transfer (SMRT) model. SMRT uses snow microstructure characteristics (density, grain size and shape, and arrangement, i.e., the interparticle distance in the microwave range linked to the grain aggregation) to drive electromagnetic models (EMs) to compute the scattering and absorption coefficients in snowpack layers [26]. Two recent modifications in SMRT could help further improve modeling the complex arctic snowpack: 1) a new concept of snow microstructure parameter named "microwave grain size" was proposed in Picard et al. [24] using a polydispersity factor which scales heterogeneity within the microstructure and 2) the symmetrized strong contrast expansion (SymSCE) EM allowing a continuous scattering coefficient formulation across the full-density range [35] to help model high density snowpacks (400–600 $kg\,m^{-3}$). The challenge regards this transition zone between hard snow to icy snow.

To test these two modifications, we evaluated SMRT simulations driven from snow properties measured in situ and compared simulations with surface and satellite radiometer observations at 19, 37, and 89 GHz. Different experimental settings and sites were considered. We first looked at snow slabs isolated or extracted from the remaining of the snowpack which limits the influence of other features (soil and other snow layers), subject to high uncertainties. We then analyzed the emission of entire snowpack–soil emissions to complete the validation. The slab datasets used in this study are independent of the previous study on the microwave grain size done by Picard et al. [25]. The slabs come from three datasets: taiga snow from Finland [13]; Canadian Arctic snow (this study and [36]); and snow from continental Antarctica considered as a slab to test high density snow [8], [23]. Validations for full snowpack were performed using surface-based and satellite-based observations over Canadian Arctic sites.

This article is structured in four parts: 1) we first studied the optimal parametrization of the microstructure for two EMs improve Born approximation (IBA) and SymSCE for homogeneous snow slabs extracted from natural seasonal snowpack; 2) the problem of high-density snow was then investigated by including three additional sites from Antarctica and looking at IBA and SymSCE biases with observations; 3) we validated these results on an independent dataset of multilayer snowpack with surface-based radiometer measurements (19, 37, and 89 GHz); and 4) with satellite-based brightness temperature observations (19 and 37 GHz).

II. Data and Models

A. Snow Data and Radiometric Measurements

Two types of surface-based radiometer measurements were used in this study. The first was collected over homogeneous snow slabs extracted from snowpack in order to avoid the complexity of microwave interactions between multiple layers, and the second over natural snowpacks (measuring the snowpack overlaying the soil). Microwave data and the snow properties needed for model simulations were collected during different field campaigns generally at the end of the snow season before the melting season (March or April in the Arctic) in open areas
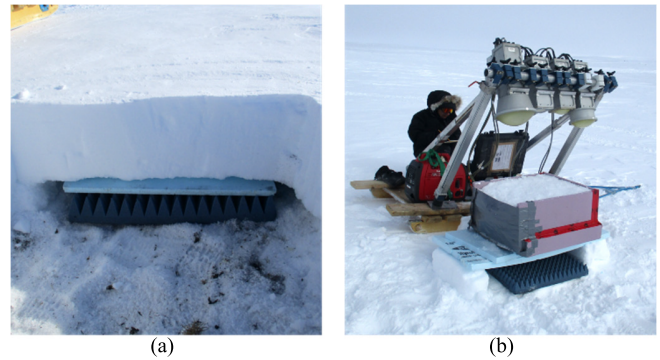

(a)   (b)

Fig. 1.   2022 slab experiments in Cambridge Bay, NU, Canada. (a) WS with the absorber put in the hole under the WS. (b) DH layer shoveled in a polystyrene foam box put over the absorber. The set was positioned in the field of view of the mobile microwave radiometers on a sled. The sled was moved so that each frequency was looking at the sample.

at several sites in taiga environment in Finland and from Arctic sites in Northern Canada (see Table I).

For the slab experiments at each site (see Section III-A), the samples were cut from the snowpack with a metal plate and carefully extracted to preserve the snow structure following Wiesmann et al. [40] (see also [13], [36]). The ∼15-cm thick extracted samples were gently put over a microwave-transparent 3-cm thick polystyrene foam (Styrofoam) sample holder above an absorber (ECOSORB[1] absorber with emissivity ∼1) in front of the radiometer field of view. In contrast, during the Cambridge Bay 2022 field campaign, we dug under the WS (which was very hard) to eliminate the DH and insert the Styrofoam [see Fig. 1(a)]. To extract the DH layers, the noncohesive crystals were scooped up and put into a Styrofoam box [see Fig. 1(b)]. Doing so disturbed the layer structure, but this was the only practical way to extract a thick (15 to 25 cm) and homogeneous layer of hoar crystals. The Cambridge Bay (Nunavut, Canada) slab dataset includes six slabs classified as WSs and six as DH (see Tables I and II). During the 2016–2017 winter at the Umiujaq (Northern Québec, Canada) sites, we extracted six WSs and four DH samples (see Table I). For the Sodankylä, Finland site, the dataset from the Arctic Snow Microstructure Experiment (ASMEx), which took place in the winter of 2014–2015, includes eight WSs and four DH samples (see Table I).

For each experiment (snowpack and slab) at Umiujaq and Cambridge Bay sites (see Table I), several snow physical properties were measured: density, physical temperature, surface specific area (SSA), and grain type, every 3 or 5 cm along the snow pit wall. The physical temperatures were measured from a probe thermometer (±1 K). The density profiles were recorded using a density cutter with a volume of 100 or 250 cm^3. The SSA measurement were done using the shortwave infrared reflectometry [2], [6].

We conducted a visual stratigraphy assessment of the main snow layers/features, including ice lenses and type of snow grain morphology following the international classification [9]. The absorbing material and air physical temperatures were also measured during the experiments. The mean snowpack properties of the new 2022 Cambridge Bay dataset appear in Table II.

[1]Trademarked.

TABLE I

DATA USED IN THIS STUDY, INCLUDING THE MEAN SNOW DEPTH (SD), THE NUMBER OF SNOW PITS (NO. OF PITS FOR THE BULK SNOWPACK EXPERIMENT), AND OF ISOLATED SNOW SLAB EXPERIMENTS (SLAB EXP.). DETAILS ON FIELD CAMPAIGNS APPEAR IN REFERENCES. THE SECTIONS CORRESPONDING EACH DATASET APPEAR IN THE "SECTIONS" COLUMN

Sites	Years	Lat/Lon	Types of snow	SD (cm)	Pits	Slab exp.	Freq (GHz)	View angle	References	Sections
Umiujaq, QC, Canada	2016–2017	56° N/ -76° W	Subarctic Tundra	12	- -	10	19,37,89	55°	i	A-B
Cambridge Bay, NU, Canada	2022 2022 2015–2019	69° N/ -105° W	Arctic Tundra	34 45 36	- 14 248	12 - -	19,37,89 19,37,89 19,37	20°,55° 20°,55° 55°	ii ii vi	A-B C D
Trail Valley Creek, NWT, Canada	2018–2019	68° N /-133° W	Arctic Tundra	42	68	-	19,37	55°	vi	D
Sodankylä, Finland	2014–2015	67° N/27° E	Taiga	15	-	14	18.7,21, 36.5,89, 150	50°	iii	A-B
Dome C/Cap Prud'homme, Antarctica	2012	75° S/123° E 67° S/134° E	Continental Ice	800 ∞	2	- - 1	19,37	55°	iv v	A-B A-B

i: Vargel et al. [36]; ii: This study; iii: Maslanka et al. [13]; iv: Picard et al. [23]; v: Dupont et al. [8], vi: Meloche et al. [20].

TABLE II

MEAN SNOW PROPERTIES AND VARIABILITY ($\pm\sigma$) FOR THE 2022 CAMPAIGN IN CAMBRIDGE BAY, NU

Cambridge Bay 2022	Snow type	Density ($kg\,m^{-3}$)	SSA ($m^2\,kg^{-1}$)	Temp (K)	Thickness (cm)
Slab experiment	WS	436.5±57.1	14.1±3.4	255.3	43.6±39.7
	DH	249.1±5.3	9.3±0.5	254.6	24.6±4.7
Full snow pit	WS	389.9±75.4	16.1±9.1	254.8	27.9±37.6
	DH	265.3±64.9	8.5±1.5	257.2	16.8±9.4

Three additional points are from Antarctica; they were acquired during an austral summer field campaign in January 2012 (see Table I). The first one was taken over blue ice at Cap Prud'homme, east Antarctica (near the French coastal station of Dumont d'Urville). The ice with many apparent bubbles had a measured surface density of 850 ± 10 kg m^{-3}, and is considered here as homogeneous over a thickness of some ten meters and a mean bubble radius of 0.52 ± 0.23 mm (SSA was derived from the mean bubble radius measured on a sample as detailed in [8, Fig. 10]). The bubbles were visually spherical and of the same diameter. The two other snow pits (named SP1 and SP2) were near the Concordia station, east Antarctica, with contrasted brightness temperatures due to different hardness: hard (SP1) and very hard (SP2) [23]. The density profiles were measured down to 8 m on snow cores sliced every 5 cm with a miter saw. The height and diameter of each sample were measured with a caliper to deduce the volume assuming a cylindrical shape. The mass was measured with a precision scale. The density profiles show that the SP1 snowpack upper part has a density value of 390 kg m^{-3}, while SP2 has a density of 410 kg m^{-3}, on average, in the first meter. The snow grain size was measured in the same boreholes using the profiler of snow specific surface area using shortwave infrared reflectance measurement (POSSSUM), (see [2]). The temperature profile was recorded about 1 km away, near Concordia Station using a string of 40 temperature probes from the surface to 20 m depth [23]. The possible spatial variation in snow temperature is assumed negligible as this site is very homogenous (same albedo, altitude, and a slope almost nil) leading to similar meteorological forcing at this scale.

A final dataset from the Canadian Arctic (Cambridge Bay, 2015–2019, and Trail Valley Creek, Northwest Territories, 2018–2019) was also used has an independent evaluation with satellite observation. The simulation is based on a two-layer model (WS/DH). The dataset comes from Meloche et al. [20] with mean snow properties for both WS (SSA: 20 m^2 kg^{-1}, Density: 335 kg m^{-3}) and DH (SSA: 11 m^2 kg^{-1}, Density: 266 kg m^{-3}). Brightness temperatures were simulated using the fixed DH fraction (DHF) (DHF = 0.46) and mean snow depth for each year and location (see [20, Table VI]).

The surface-based microwave brightness temperature (T_B) measurements were acquired in both vertical (V-pol) and horizontal (H-pol) polarizations at incidence angles of 20° to 50°/55°, and at frequencies of 150, 89, 37/36.5, 21, and 19/18.7 GHz depending on the experiments. Table I references detailed measurements and methods. Satellite observations for Cambridge Bay and Trail Valley Creek were from the Special Sensor Microwave/Imager and Sounder (SSMIS) sensor at 37 and 19 GHz, with the Equal-Area Scalable Earth (EASE)-Grid 2.0 resampled at 3.125 km (6.25 km for 19 GHz) resolution [3], see Meloche et al. [20] for more details on processing. For Cambridge Bay and Trail Valley Creek T_B simulations, soil permittivity and roughness were derived from a previous study [19] based on a semi-empirical rough soil reflectivity model [39]. The frozen soil permittivity value was $\epsilon = 3.36 + 0.002i$ and roughness $\sigma_h = 1.7$ cm. The downwelling atmospheric radiation ($T_{B,\mathrm{atm}}$, γ_{atm}) were also estimated from atmospheric modeling [36] and then used in SMRT, except for Sodankylä's dataset where it was measured directly. The brightness temperature measurements were then compared to the simulated brightness temperature from the SMRT.

B. SMRT Model

The SMRT model [26] has recently been improved to provide a consistent theoretical treatment for passive microwave simulations based on the snow microstructure representation for each layer defined by three parameters: the density, the SSA, and the microwave polydispersity (K) [25]. The three parameters are measurable and can be used for any common
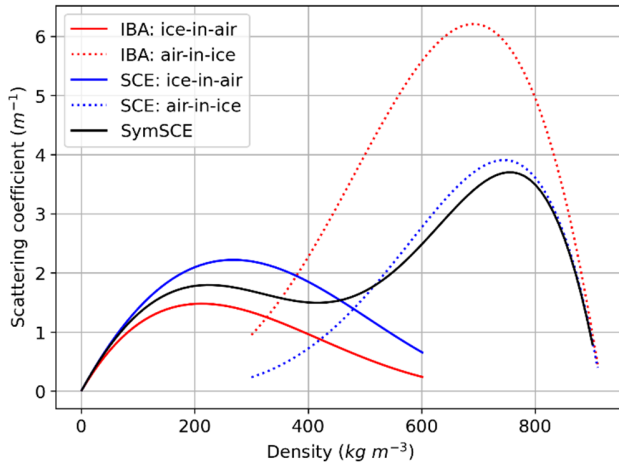
Fig. 2. Variation of scattering coefficient as a function of density using the SMRT SCE (blue), the SymSCE (black), and the IBA (red) models for both media, snow, and bubby ice (see text). Simulations are at 37 GHz for a theoretical homogeneous porous medium with SSA = 15 m² kg⁻¹, $K_{snow} = K_{ice} = 1$, and Temperature = 263 K. The microstructure model is exponential with correlation length defined by (2a) and (2b) for, respectively, ice-in-air (snow) and air-in-ice (bubbly ice).

microstructure type (e.g., exponential and sticky hard sphere). The polydispersity can be estimated from the microcomputed tomography measurement of the snow 3-D chord length distribution (see [25, Eq. (8)]). As tomography was not available for the sites in this study, K was retrieved by minimizing the difference between microwave measurements and simulation.

The EM computes the scattering and absorption coefficients in each snow layer. Here, we tested the nonlocal (i.e., where averaged polarization field at a given point is assumed to depend on the average electric field at other localities), strong contrast expansion (SCE) theory for heterogeneous porous dielectric media, rigorously accounting for complete microstructural information (infinite set of n-point correlation functions) and hence multiple scattering [35]. Picard et al. [24] recently implemented SCE model in SMRT. SCE allows computing effective wave propagation and scattering coefficients in any random two-phase medium. In our case, two media are considered: snow represented by ice particles in a background of air (ice-in-air mixture) and bubbly ice represented by air bubbles embedded in ice (air-in-ice mixture). Considering the ice fraction of the medium ($\phi_{ice} = \rho_{medium}/\rho_{ice}$), the snow representation is typically valid for an ice fraction of 0–0.3 and the bubbly ice for 0.7–1. The symmetrization of SCE model [35] (labeled SymSCE) is based on the combination of the polarizabilities of each medium (a function of dielectric constant) weighted by $1 - \phi_{ice}$ and ϕ_{ice} for the snow (ice-in-air) and inverted (air-in-ice) media, respectively (see [35, Eq. (D1)]). This allows to continuously cover the critical zone between $\phi_{ice} > 0.3$ and $\phi_{ice} < 0.7$, given a higher weight to the snow at low ϕ_{ice} and to the bubbly ice at high ϕ_{ice} (see Fig. 2). This allows an approximate approach, computationally efficient and physically rigorous, to continuously cover the critical zone between $\phi_{ice} > 0.3$ and $\phi_{ice} < 0.7$ (see Fig. 2).

The way scattering function accounts for geometrical characteristics of the medium microstructure is the same in SymSCE and IBA models. The microstructure information is

carried by the "microwave grain size" parameter

$$L_{MW} = K_{medium} \times L_{p,medium} \tag{1}$$

where K_{medium} is the polydispersity and $L_{p,medium}$ is the correlation length (also called Porod length). The latter can be calculated as [17] and [24], for ice-in-air

$$L_{p,\text{ice-in-air}} = 4\frac{(1 - \phi_{snow})}{(\rho_{ice}SSA)} = 4\frac{(1 - \rho_{snow}/\rho_{ice})}{(\rho_{ice}SSA)} \tag{2a}$$

and for air-in-ice medium

$$L_{p,\text{air-in-ice}} = 4\frac{\phi_{snow}}{(\rho_{ice}SSA)} = 4\frac{(\rho_{snow}/\rho_{ice})}{(\rho_{ice}SSA)}. \tag{2b}$$

The SymSCE scattering coefficients are compared to the IBA scattering coefficient assuming $K_{snow,ice} = 1$ in Fig. 2. A discontinuity indeed appears in the critical transitional zone between snow and ice when respectively using $L_{p,snow}$ [see (2a)] and $L_{p,ice}$ [see (2b)] for defining their microstructural parameter.

Physically, the scattering coefficient increases with the number of scatterers (i.e., the fractional volume) and with the randomness in the medium. As the scatterers are more and more packed, the randomness decreases because the scatterer positions are more and more constrained by the others and this effect is stronger than the effect of increasing scatterer number at high fractional volume. This results in a maximum of scattering somewhere at intermediate fractional volume, and in a bell-shaped curve. In the setting where air and ice are switched, we have in fact two bell shaped curves with two local maximums (see Fig. 2). Noting that these maximums are at relatively low and high densities, respectively, a local minimum must exist in the middle range, mathematically. Physically this can be understood as a stage where packing strongly constrained the position of the scatterers. However, it is worth noting that this local minimum is very shallow, and it depends on the precise shape of the curves which themselves depends on the packing model (the microstructure model) and on where the switch is performed. Therefore, the position and the depth of this minimum is certainly variable for real snow.

For the snow or ice-in-air mixture, the SCE and IBA scattering coefficients are similar, while for the air-in-ice mixture, the SCE scattering is lower than for the IBA. Based on IBA, the exponential spatial autocorrelation function proposed by Mätzler and Wiesmann [15] gave good results in its experiment with coarse-grain crusts growing and decaying during melt-and-refreeze cycles, reaching layers of densities up to 700 kg m⁻³. For IBA, the scattering coefficient of ice-in-air between 300 and 600 kg m⁻³ density appears clearly lower compared to that of air-in-ice at the same densities. For SCE, this occurs at a density above ∼500 kg m⁻³. For 37 GHz at 458.5 kg m⁻³ (i.e., at $\phi_{snow} = \phi_{ice} = 0.5$) using IBA, $\kappa_{s,snow} = 0.7$ m⁻¹ is substantially lower compared to $\kappa_{s,ice} = 3.3$ m⁻¹ (see Fig. 2). The theoretical SCE-snow and SCE-ice curves intersect at $\kappa_{s,snow} = \kappa_{s,ice} = 1.3$ m⁻¹ for 470 kg m⁻³, while those from IBA intersect at $\kappa_{s,snow} = \kappa_{s,ice} = 1.1$ m⁻¹ for 330 kg m⁻³. The SymSCE curve for which κ_s varies continuously in the transition zone is also shown for comparison (black line, Fig. 2).

In the IBA EM model, the field ratio accounting for the difference in the electric field inside the scatterers of relative dielectric permittivity ε_2 and the background ε_1 is a function of ε_1, ε_2 and the effective permittivity of the medium (see [15, Eq. (2)]). This field ratio is the only term in the IBA equations that changes when switching from ice-in-air to air-in-ice microstructure (i.e., $\varepsilon_1 \rightarrow \varepsilon_2$, $\varepsilon_2 \rightarrow \varepsilon_1$, $f \rightarrow 1 - f$) and poses a very significant change (e.g., from 0.48 to 2.06 at $f = 0.5$, [15, Eq. (2)]). All the other terms are unaffected by this switch, and they are invariant. IBA hence features a much stronger air-in-ice scattering than the ice-in-air at the same fractional volume of scatterers.

The SCE model also presents a stronger scattering in the air-in-ice than in the ice-in-air, but shows a lesser amplitude than for IBA. SCE formulation does not involve the field ratio. The explanation rather lies in the effective permittivity difference between low- and high-density media. In the air-in-ice medium, as the wave propagates in a medium with a higher permittivity than in ice-in-air medium, its wavelength is shorter than in air (by a factor $(\varepsilon_{\mathrm{medium}})^{1/2}$ between 1 and $\sim$1.77 for pure ice). The apparent size of the scatterers is therefore seen larger by the wave, leading to a stronger scattering in the air-in-ice side. Rayleigh scattering is indeed proportional to the volume of the scatterers relative to the wavelength. Note that IBA is also subject to this effect, in addition to the field ratio effect. Beyond the limit of $\sim$800 $\mathrm{kg\,m^{-3}}$, the number of scatterers per unit volume decreases in the medium, which becomes pure ice, decreasing the scattering coefficient. Nevertheless, absorption continues to increase so that the single scattering albedo decreases, and the brightness temperature increases as a result [22], [26], [30].

The SymSCE model is based on the "nonlocal" SCE formalism and has been symmetrized [24], [35]. The result is that SymSCE formulation is unaffected when switching from ice-in-air to air-in-ice microstructure. However, we still see a stronger scattering for higher density, for the same reason as for SCE.

In the following, the IBA (both media) and SymSCE were used for all T_B simulations.

III. RESULTS

A. Slab Experiments

The comparisons between measured and simulated brightness temperatures during the isolated slab experiments (wind pack slabs and DH slabs) for all sites appear in Fig. 3 (Cambridge Bay, CB; Sodankylä, SK; Umiujaq, UMI; Dome C, Antarctica, DC) for both IBA and SymSCE models. The polydispersity values (K) minimizing the root mean square error (RMSE) in each case appear in Table III. Results show that, for the IBA$_{\mathrm{ice-in-air}}$ model, the retrieved WS polydispersity K_{WS} ranges from 0.76 to 0.84 if considering the sites separately (see Table III), with a mean value of $K_{\mathrm{WS}} = 0.80$ for all sites. Note that the minimization in Umiujaq site did not converge. We believe this is due to the extracted slabs being almost transparent at 19 and 37 GHz due to a combination of small thickness and grain size. This is not the case for DH since the scattering due to large grain size is significant. When using the SymSCE model, the polydispersity coefficient K_{WS}
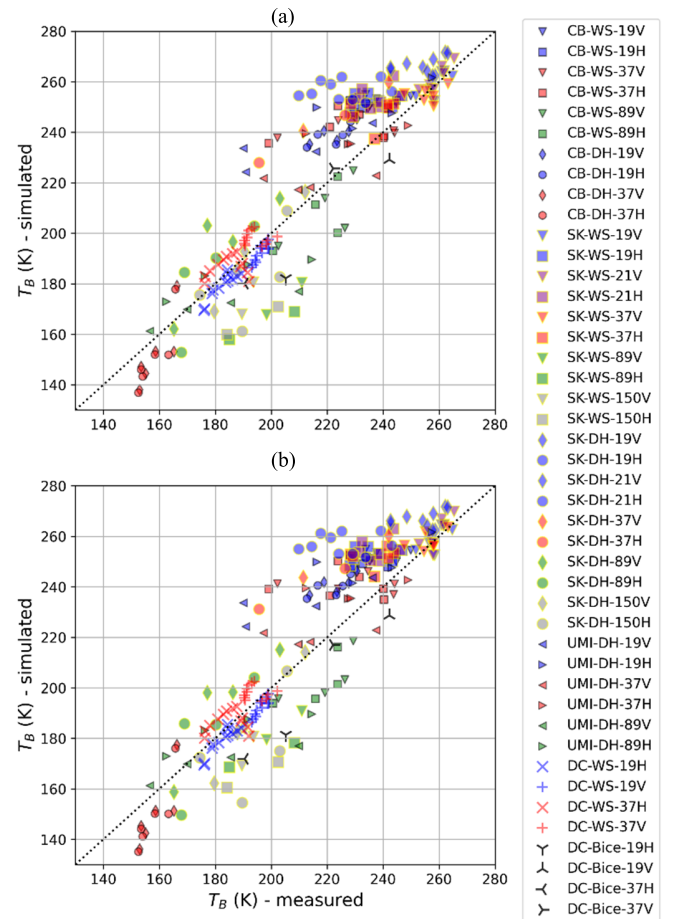

Fig. 3. Simulated and measured brightness temperatures for all slab experiments (Wind slab, WS; depth hoar, DH) and bubbly ice (Bice), both polarization (vertical, V, and horizontal, H) and all frequencies used with effective polydispersity from Table III. (a) IBA model with RMSE = 13.4 K, Bias = 4.3 K, and $R^2 = 0.87$ and (b) SymSCE model with RMSE = 14.0 K, Bias = 4.3 K, and $R^2 = 0.86$.

TABLE III
EFFECTIVE MICROWAVE POLYDISPERSITY COEFFICIENT FOR EACH TYPE OF SNOW (WS: WIND SLAB; DH: DEPTH HOAR; BICE: BUBBLY ICE), FOR EACH SITE (SK: SODANKYLÄ; CB: CAMBRIDGE BAY, NU; UMI: UMIUJAQ, QC; DC: CAP PRUD'HOMME, ANTARCTICA), AND FOR EACH MODEL (IBA$_{\mathrm{ice-in-air}}$, IBA$_{\mathrm{air-in-ice}}$, AND SYMSCE)

		SK	CB	UMI	DC	Mean
WS	IBA$_{\mathrm{ice-in-air}}$	0.84	0.81	-	0.76	**0.80**
	SymSCE	0.73	0.67	-	0.63	**0.68**
DH	IBA$_{\mathrm{ice-in-air}}$	1.28	1.36 (1.2–1.5)	1.34 (1.1–1.6)	-	**1.33**
	SymSCE	0.95	1.22	1.07	-	**1.08**
Bice	IBA$_{\mathrm{air-in-ice}}$	-	-	-	0.70	
	SymSCE	-	-	-	0.67	

ranges from 0.63 to 0.73 (see Table III), with a mean value of 0.68, that is about 15% lower than IBA.

For the isolated DH slabs, results show that, for the IBA model, the retrieved polydispersity coefficient K_{DH} ranges from 1.28, 1.36 to 1.34, respectively, for SK, CB, and UMI sites (see Table III). In the cases of CB and UMI, the
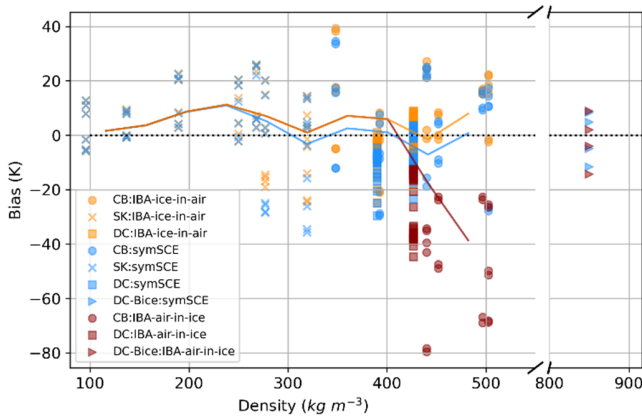
Fig. 4. Bias in brightness temperature (K) (simulated mean TB at 19 and 37 GHz and both polarizations minus measured) of WS as a function of density. The lines represent the rolling average of the different EM models. Slabs with a density over 400 $kg\,m^{-3}$ appear in red using an inverted medium. A constant polydispersity of 0.76 (mean of WS) was used for all simulations.
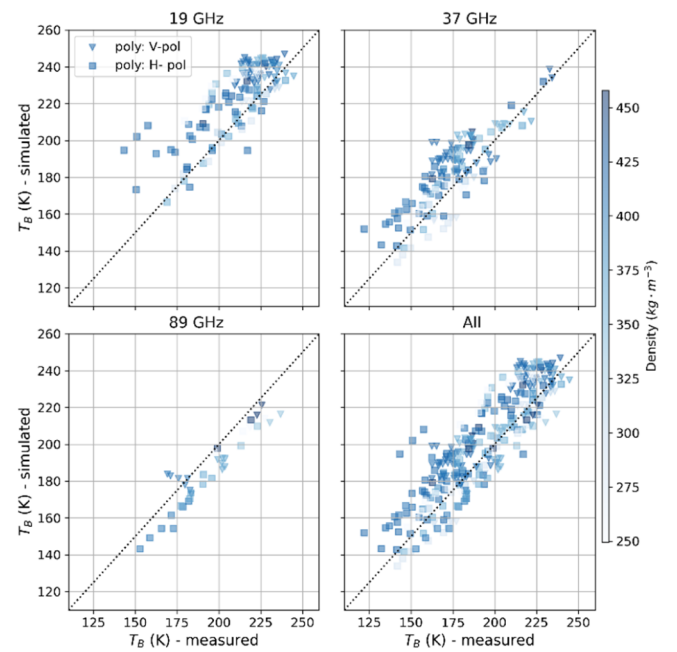

Fig. 5. Simulated and measured brightness temperatures for the 2022 Cambridge Bay snow pit experiments by frequencies and all frequency together using IBA model with values of polydispersity $K_{WS} = 0.80$ and $K_{DH} = 1.33$. Color graduation is a function of each pit mean snow densities.

convergence is relatively flat without significant variation of the RMSE (± 1 K) between 1.2–1.5 and 1.1–1.6, respectively (see Table III). Thus, the mean K_{DH} value was 1.33. For the SymSCE model, K_{DH} varies from 0.95, 1.22, and 1.07, respectively, for SK, CB, and Umi sites (see Table III), with a mean of 1.08, that is 19% lower than IBA.

The bubbly ice sample (Bice), with retrieved K values of 0.70 and 0.67, respectively, for $IBA_{air-in-ice}$ (RMSE = 8.7 K) and SymSCE models (RMSE = 7.9 K) (see Table III), are close to the K_{WS} values, in agreement with the observed small air bubbles size.

The effective polydispersity derived from the fit between simulated and measured microwave brightness temperatures slightly depends upon frequencies due to the vertical inhomogeneity of the slab and the frequency-dependent penetration depth. It is thus difficult to determine which frequencies are the best, without independent comparison with micro-CT K values (see Section IV).

B. Density Evaluation

To assess IBA and SymSCE behaviors for high density snow, we analyzed the results (bias) for WSs as a function of densities (see Fig. 4).

The mean bias between simulated and measured T_B does not substantially change with density between 400 and 500 $kg\,m^{-3}$ for SymSCE and $IBA_{air-in-ice}$ (Fig. 4, blue and yellow points, respectively). When we inverted the medium to air-in-ice using IBA for slabs with density >400 $kg\,m^{-3}$ (Fig. 4, $IBA_{ice-in-air}$, red points), we see an increase (negatively) in the bias between simulated and measured T_B. Such behavior agrees with the scattering coefficient variations shown in Fig. 2. The scattering using the inverted medium with IBA ($IBA_{ice-in-air}$) seems to overestimate scattering. Note that in Fig. 4, we used a constant polydispersity value ($K = 0.76$) for all models. If the optimized values of K (see Table III) were used, the difference between SymSCE and $IBA_{air-in-ice}$ would be smaller since the lower K for SymSCE and higher K for $IBA_{air-in-ice}$ would compensate for the difference in scattering between both models.

C. Validation of the Arctic Snowpack

In Section III-B, we determined an effective microwave polydispersity retrieved from the slab experiments. Here, we assess the usefulness of these values applied to an independent dataset of natural Arctic snowpacks collected at Cambridge Bay in April 2022 (see Tables I and II). In Table IV, the first column shows the result using the measured SSA and density of each layer and the K values optimized from the previous section (slab experiment). For the IBA simulations, we used $K_{WS} = 0.80$ or $K_{DH} = 1.33$, and for SymSCE simulations $K_{WS} = 0.68$ or $K_{DH} = 1.08$. Results appear in Figs. 5 (IBA) and 6 (SymSCE) per frequency. Positive biases were higher at 19 GHz (11.9 K for IBA and 14.8 K for SymSCE) (see Table IV) compared to 37 GHz (7.5 K for IBA and 11.7 K for SymSCE). Negative biases were observed at 89 GHz. The second column in Table IV shows the results of K that minimized the natural snowpack dataset RMSE. This allowed the best outcome in terms of RMSE for K to be determined and compared with values from the K derived in the slab experiment.

The third column in Table IV shows results using an empirical scaling factor ϕ for the optical radius of the snow grains as done in previous studies [27], [36].

With the IBA, using the mean polydispersity values derived from the slab experiments and applied for the full snow pits yields an RMSE ranging from 17.5 to 11.3 K depending on frequency and with the SymSCE, from 19.6 to 13.7 (+10%) (Table IV, first column). These values are slightly higher (+20%) than those derived by optimizing the natural snowpacks (Table IV, second column). Hence, using average values of polydispersity parameters for WS and DH does not alter the simulations too much; therefore, this approach allows simulation of Arctic snowpack emissivity and remains valid

TABLE IV
RMSE, Biasm, and Correlation Coefficient (R^2) Between Simulated and Measured (Ground-Based) T_B at Cambridge Bay 2022 for Both EM Models (IBA and SymSCE) Using K Optimized With the Slab Experiments (see Section III-A), Using K Optimized for the Snow Pit Layer, and Using a Single Scaling Factor for Both WS and DH Snow Types (ϕ)

| RMSE, Bias R^2	K Optimized by slab		K Optimized by snow pit layer		ϕ Optimized scaling factor	
	IBA $K_{WS} = 0.80$ $K_{DH} = 1.33$	SymSCE $K_{WS} = 0.68$ $K_{DH} = 1.08$	IBA $K_{WS} = 0.56$ $K_{DH} = 1.66$	SymSCE $K_{WS} = 0.47$ $K_{DH} = 1.41$	IBA ($\phi = 1.44$)	SymSCE ($\phi = 1.22$)
TB 19 V-H	17.5 K, 11.9 K 0.61	19.6 K, 14.8 K 0.62	14.2 K, 5.1 K 0.60	15.0 K, 7.4 K 0.61	16.0 K, 6.9 K 0.53	16.9 K, 9.1 K 0.54
TB 37 V-H	13.8 K, 7.5 K 0.70	17.2 K, 11.7 K 0.65	10.8 K, -3.2 K 0.78	11.9 K, -4.4 K 0.75	15.6 K, -5.2 K 0.53	15.9 K, -4.5 K 0.49
TB 89 V-H	11.3 K, -8.6 K 0.88	13.7 K, -11.5 K 0.88	7.7 K, -1.8 K 0.91	8.7 K, -4.1 K 0.91	24.6 K, -22.2 K 0.79	29.8 K, -27.0 K 0.69
All freq.	**15.3 K, 7.5 K 0.78**	**17.9 K, 10.3 K 0.73**	**12.1 K, 0.6 K 0.83**	**13.0 K, 0.8 K 0.82**	**17.1 K, -2.0 K 0.69**	**18.6 K, -1.3 K 0.65**
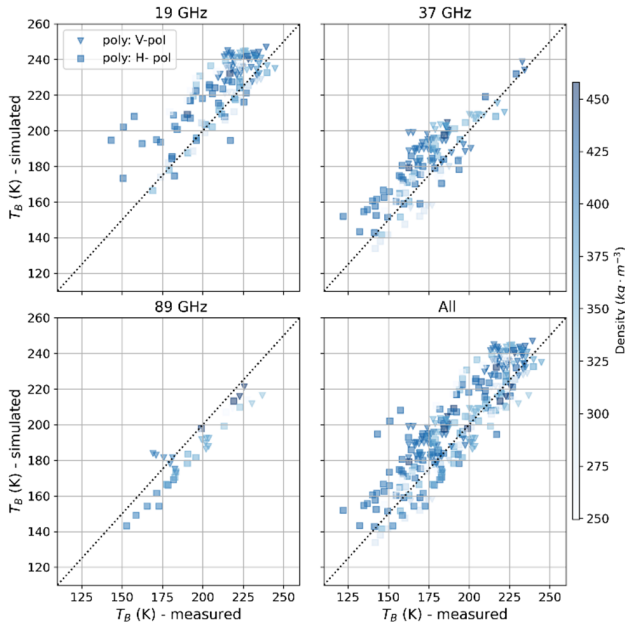
Fig. 6. Same as Fig. 5, but for SymSCE simulations with polydispersity values $K_{WS} = 0.68$ and $K_{DH} = 1.05$.

for generalization to a certain extent. Moreover, even though, theoretically, there should be no frequency dependence of the errors, differences do appear (greater RMSE at 19 GHz) (see Table IV). This may be due to the contribution of ground scattering under the snow, which is greater at 19 than at 89 GHz because of the greater emission depth at 19 GHz. Also, as mentioned for the slab experiment, no trend appears in RMSE as a function of density or SSA.

At last, we tested the hypothesis of using an empirical scaling factor ϕ for the snow grains optical radius. This is equivalent to assuming a single value of polydispersity for all snow types. Results show an increase in mean RMSE of 2 K (w/r optimized by slabs, col. 1) and 5 K (w/r optimized by snow pit layer, col. 2) (see Table IV). Particularly at 89 GHz, the significant RMSE difference between the polydispersity approach (7.7 and 8.7 K) and the mean scaling factor (19.1 and 27.1 K) clearly demonstrates that considering

the polydispersity by grain type is a major improvement over the previous scaling factor.

D. Validation Using Satellite Observations

For practical purposes, regarding the satellite SWE retrieval, we assessed the effect of polydispersity on satellite observation simulations using Meloche et al. [20] dataset. Assuming an Arctic snowpack with a fixed fraction of WS and DH layers (observed mean DHF = 46%), we simulated T_B for multiple years and for two Arctic sites [20]. We also used mean values of SSA and density for each WS and DH layer. We compared the error metrics (RMSE and R^2) obtained using either the polydispersity values for the slab experiment (Table IV, column 1) or a scaling factor for the optical grain size (Table IV, column 3). For satellite-based measurements (see Table V), we also found that for, both models at 37 GHz, the RMSE is better when using two polydispersity values than when using the scaling factor (for IBA: 11.8 K compared 21.2 K; for SymSCE: 9.3 K compared to 16.4 K, Table V), while it is not the case at 19 GHz. It is likely that, at 19 GHz, where the penetration depth is greater and therefore the ground emission contribution is much higher, the scaling factor optimization also compensates for the ground emission uncertainty, in addition to snow scattering. In the case of polydispersity approach, there is no optimization.

This means that the proposed approach using generic mean values of snow properties (see [20, Fig. 5]) for Arctic snowpack with a two-layer stratification could be applied to simulate satellite-based observations. For IBA, 37 GHz yields a significant improvement with a 44% lower RMSE (from 21.2 to 11.8 K) using two polydispersity values.

IV. DISCUSSION

For the two types of snow (WS and DH) analyzed in this study, the values of microwave polydispersity derived from surface-based microwave radiometry well agree with those found in Picard et al. [25]. Particularly noteworthy is that the polydispersity values found in this study with IBA for Arctic WSs (0.8) very closely match the range of values from

RMSE, R²	Polydispersity (K_{WS}, K_{DH})		Scaling factor	
	IBA $K_{WS} = 0.80$ $K_{DH} = 1.33$	SymSCE $K_{WS} = 0.68$ $K_{DH} = 1.08$	IBA ($\phi = 1.44$)	SymSCE ($\phi = 1.22$)
TB 19 V-H	11.8, 0.74	14.5, 0.75	9.4, 0.75	11.5, 0.76
TB 37 V-H	11.8, 0.52	9.1, 0.52	21.2, 0.53	16.4, 0.53
All freq.	**11.8, 0.63**	**11.8, 0.63**	**15.3, 0.64**	**14.0, 0.65**

TABLE VI

SUMMARY OF POLYDISPERSITY VALUES ESTIMATED IN THIS STUDY (*) AND REPORTED BY PICARD ET AL. [25]

Type of snow	Method	Polydispersity K
Sphere	Theory	0.4
Bubbly ice*	MW	0.7
Antarctic*	MW	0.67
Alpine WS	mu-CT	0.6-0.9
Arctic WS*	MW	0.8
Alpine DH	mu-CT	0.7-0.9
Finnish DH	mu-CT	0.8-1.2
Arctic DH	MW	1.2-1.8
Arctic DH*	MW	1.33
Debye Random medium	Theory	1

laboratory microcomputer tomography (μ-CT) measurements for Alpine WSs (0.6–0.9). The same is true for the Finnish DH polydispersity in this study (SymSCE: 1.08, IBA: 1.28) with respect to the range of μ-CT measurements (0.8–1.2) (see Table VI). Regarding the Arctic DH, for which no μ-CT measurements yet exist, the value found by microwave retrieval in this study (1.33) from isolated DH layers also well corresponds to the range (1.2–1.8) found by Picard et al. [25] from an independent dataset (see Table VI).

During the Sodankyla's ASMEx experiment [32], the μ-CT-derived exponential correlation length $l_{ex}(x, y, z)$ and the Debye correlation length $l_p(x, y, z)$ based on μ-CT-derived SSA and density were estimated. We estimated the approximate polydispersity of each AMSEx's slab samples by using the following approach using mean (x, y, z) values: $K_{approx} = l_{ex}/l_p$. This equation of K_{approx} differs from the true (8) suggested by Picard et al. [25] for estimating K and comparison should be interpreted with care. Here, we compared K_{approx} with K_{MW} estimated from microwave measurement but with $l_p(x, y, z)$ based on μ-CT-derived SSA and density (with respect to earlier in this article where optical-derived SSA was used). Substantial overestimation of the SSA from the optical method compared to the μ-CT can be observed [13] which influence the final K_{MW} in our case. We believe that the difference between SSA estimation by the optical methods

compared to SSA by a micro-CT is not only related to DH but all grain type [13]. This topic is beyond the scope of this article, and merits more in-depth investigations. Results show that K_{approx} is similar to K_{MW} using IBA for the WS ($K_{approx} = 0.64$ compared to $K_{MW} = 0.62$ using IBA and $K_{MW} = 0.51$ using SymSCE), while the K_{approx} value is closer to the K_{MW} SymSCE value for the DH slab ($K_{approx} = 0.76$ compared $K_{MW} = 1.06$ using IBA and $K_{MW} = 0.68$ using SymSCE).

Note that the approach of retrieving the polydispersity by optimization could compensate for different uncertainties in snow measurements (spatial variability and sensor calibration). The slab experiment is difficult to carry out in the field, and is certainly subject to several sources of uncertainties, as outlined in previous studies [13], [36], [40]. Among them, the downward environmental contributions from the surroundings reflected by the slab could significantly contribute to the measured signal. Also, the possible misalignment of the antennas regarding the slab position could generate errors. At last, the limited size of the box where the snow slab is stored weakens the assumption of the ideal infinite layer, as the edges are susceptible to produce multiple reflections, contributing to the signal as well. This latter effect is most likely reduced for measurements over an isolated (instead of extracted) layer within the snowpack, as shown in Fig. 1(a). The quantification for these errors needs further investigation with improved experimental settings.

SymSCE did not yield a significant improvement compared to IBA. The only difference was the smaller polydispersity consistently found for SymSCE which compensates for the higher scattering in SymSCE compared to IBA for snow (see Fig. 2). Further investigations are needed to evaluate properly the benefit of SymSCE for hard snow while IBA simulations using inverted medium (IBA$_{air-in-ice}$) seems to increase the bias between (simulated minus measured) T_B (see Fig. 4). More physical measurements of Arctic snowpack polydispersity using micro-CT will help differentiate both model physical relevance and the correct polydispersity values.

Improvement in simulations using polydispersity for surface-based and satellite observations at 37 GHz can be noted, which is encouraging since it is the most sensitive to snow scattering, and the most promising for satellite SWE retrievals. DH crystals have always caused issues in snow emission simulation due to their high scattering properties. The simulation at 37 GHz benefits from using a two-layer snowpack with different fixed polydispersity values for WS and DH that can adjust for the scattering between these two contrasted layers. The depth of hoar layer shows a certain sensitivity on brightness temperature, as expected at 37 GHz due to its strong scattering effect. A test was carried out with the DHF set to 0.35 instead of the chosen value 0.46. RMSE increases by from 12 K (see Table V) to 20 K for both parameterization (polydispersity or scaling factor), whereas at 19 GHz, the increase in RMSE is +1.7 K. The chosen value of 0.46 is close to the best match for the sites studied [4], [10], [20], [29], [31]. But, this is an important issue as DHF increases with tundra climate-induced shrubification [31]. At 19 GHz, RMSEs between simulation and observation using

polydispersity values (without optimization) stay, however, higher compared to the approach using optimization by an empirical scaling factor as simulations could be affected by soil emission uncertainty. The fact that high frequencies (89 GHz) are more sensitive to the surface layer from which the measured TB emanates (lower penetration depth), they depend more upon the surface layer polydispersity than DH.

V. CONCLUSION

The new "microwave grain size" introduced by Picard et al. [25] was applied to multiple datasets for Arctic snow. The effective value of polydispersity for DH and WS were found using isolated slab experiments and then applied to independent datasets of surface-based and satellite microwave measurements. Effective polydispersity values agree with values found by Picard et al. [25]. The simulations of Arctic snow are found to be improved using the microwave grain size. The applicability we found so far is encouraging. The next step should focus on the measurement of physical polydispersity values of DH from microtomography instead of microwave optimization.

Moreover, we validated for the first time the scaled symmetrical SCE EM model, newly implemented in SMRT, featuring a continuously scattering transition between low and very high-density snow, including strong wind-driven compacted layers and firn up to bubbly ice. More work is, however, needed to conclude on which EM model better models the transition zone knowing the precise snow parametrization using μ-CT measurements.

The microwave grain size concept introduced a physical quantity that improved the challenging modeling of the Arctic snowpack. The scattering due to size and shape of DH is provided by high polydispersity ($K > 1$), whereas most other convex grains have a lower value ($K < 1$). This allows using a physical microstructure representation for each snow types without using empirical scaling factors as in the past but rather focusing on a parameter that can be measured and quantified per snow types. This snow polydispersity parameter could be introduced in snow microstructural representation of physical snow evolution models such as Crocus [37] or SNOWPACK [11]. Coupling improved snow model with modified RT model, such as SMRT, will thus be the next step toward global SWE retrieval from space-borne microwave observations.

ACKNOWLEDGMENT

REFERENCES

[1] J. Amlien, "Remote sensing of snow with passive microwave radiometers—A review of current algorithms," Norsk Regnesentral, Oslo, Norway, Tech. Rep. 1019, 2008, pp. 1–52.

[2] L. Arnaud et al., "Measurement of vertical profiles of snow specific surface area with a 1 cm resolution using infrared reflectance: Instrument description and validation," J. Glaciol., vol. 57, no. 201, pp. 17–29, 2011, doi: 10.3189/002214311795306664.

[3] M. J. Brodzik, D. G. Long, and M. A. Hardman, "Best practices in crafting the calibrated, enhanced-resolution passive-microwave EASE-grid 2.0 brightness temperature Earth system data record," Remote Sens., vol. 10, no. 11, p. 1793, Nov. 2018, doi: 10.3390/rs10111793.

[4] C. Derksen, J. Lemmetyinen, P. Toose, A. Silis, J. Pulliainen, and M. Sturm, "Physical properties of Arctic versus subarctic snow: Implications for high latitude passive microwave snow water equivalent retrievals," J. Geophys. Res., Atmos., vol. 119, no. 12, pp. 7254–7270, Jun. 2014, doi: 10.1002/2013jd021264.

[5] C. Derksen et al., "Development of the terrestrial snow mass mission," in Proc. IEEE Int. Geosci. Remote Sens. Symp., Jul. 2021, pp. 614–617, doi: 10.1109/IGARSS47720.2021.9553496.

[6] F. Domine, J. Gallet, J. Bock, and S. Morin, "Structure, specific surface area and thermal conductivity of the snowpack around barrow, Alaska," J. Geophys. Res., Atmos., vol. 117, no. D14, Jul. 2012, Art. no. D00R14, doi: 10.1029/2011jd016647.

[7] C. Donlon, R. Midthassel, M. Sallusti, M. Trigganese, B. Fiorelli, and C. Accadia, "The Copernicus imaging microwave radiometer (CIMR): A new view of the cryosphere," in Proc. EGU Gen. Assem. Conf. Abstr., 2022, Art. no. EGU22-11, doi: 10.5194/egusphere-egu22-11.

[8] F. Dupont et al., "Modeling the microwave emission of bubbly ice: Applications to blue ice and superimposed ice in the Antarctic and Arctic," IEEE Trans. Geosci. Remote Sens., vol. 52, no. 10, pp. 6639–6651, Oct. 2014, doi: 10.1109/TGRS.2014.2299829.

[9] C. Fierz et al., "The international classification for seasonal snow on the ground," in IHP-VII Technical Documents in Hydrology N-83, IACS Contribution N-1, UNESCO-IHP, Paris, France, 2009.

[10] J. King et al., "The influence of snow microstructure on dual-frequency radar measurements in a Tundra environment," Remote Sens. Environ., vol. 215, pp. 242–254, Sep. 2018, doi: 10.1016/j.rse.2018.05.028.

[11] M. Lehning, P. Bartelt, B. Brown, C. Fierz, and P. Satyawali, "A physical SNOWPACK model for the Swiss avalanche warning: Part II. Snow microstructuree," Cold Regions Sci. Technol., vol. 35, no. 3, pp. 147–167, 2002.

[12] J. Lemmetyinen, J. Pulliainen, A. Rees, A. Kontu, Y. Qiu, and C. Derksen, "Multiple-layer adaptation of HUT snow emission model: Comparison with experimental data," IEEE Trans. Geosci. Remote Sens., vol. 48, no. 7, pp. 2781–2794, Jul. 2010, doi: 10.1109/TGRS.2010.2041357.

[13] W. Maslanka et al., "Arctic snow microstructure experiment for the development of snow emission modelling," Geosci. Instrum., Methods Data Syst., vol. 5, no. 1, pp. 85–94, Apr. 2016, doi: 10.5194/gi-5-85-2016.

[14] C. Mätzler, "Improved born approximation for scattering of radiation in a granular medium," J. Appl. Phys., vol. 83, no. 11, pp. 6111–6117, Jun. 1998.

[15] C. Mätzler and A. Wiesmann, "Extension of the microwave emission model of layered snowpacks to coarse-grained snow," Remote Sens. Environ., vol. 70, no. 3, pp. 317–325, Dec. 1999.

[16] C. Mätzler and E. Schanda, "Scattering of electromagnetic waves by snow," J. Appl. Phys., vol. 55, no. 3, pp. 444–446, 1984.

[17] C. Mätzler, "Relation between grain-size and correlation length of snow," J. Glaciol., vol. 48, no. 162, pp. 461–466, 2002.

[18] C. Mätzler, "COST action 712: Microwave radiometry," in Remote Sensing of Atmosphere and Ocean from Space: Models, Instruments and Techniques, vol. 13. Norwell, MA, USA: Kluwer, 2002, pp. 231–246.

[19] J. Meloche, A. Royer, A. Langlois, N. Rutter, and V. Sasseville, "Improvement of microwave emissivity parameterization of frozen Arctic soils using roughness measurements derived from photogrammetry," Int. J. Digit. Earth, vol. 14, no. 10, pp. 1380–1396, Oct. 2021, doi: 10.1080/17538947.2020.1836049.

[20] J. Meloche et al., "Characterizing Tundra snow sub-pixel variability to improve brightness temperature estimation in satellite SWE retrievals," Cryosphere, vol. 16, no. 1, pp. 87–101, Jan. 2022, doi: 10.5194/tc-16-87-2022.

[21] J. Pan et al., "Differences between the HUT snow emission model and MEMLS and their effects on brightness temperature simulation," IEEE Trans. Geosci. Remote Sens., vol. 54, no. 4, pp. 2001–2019, Apr. 2016, doi: 10.1109/TGRS.2015.2493505.

[22] G. Picard et al., "Simulation of the microwave emission of multi-layered snowpacks using the dense media radiative transfer theory: The DMRT-ML model," Geosci. Model Develop., vol. 6, no. 4, pp. 1061–1078, Jul. 2013, doi: 10.5194/gmd-6-1061-2013.

[23] G. Picard, A. Royer, L. Arnaud, and M. Fily, "Influence of meter-scale wind-formed features on the variability of the microwave brightness temperature around dome c in Antarctica," *Cryosphere*, vol. 8, no. 3, pp. 1105–1119, Jun. 2014, doi: 10.5194/tc-8-1105-2014.

[24] G. Picard, H. Löwe, and C. Mätzler, "Brief communication: A continuous formulation of microwave scattering from fresh snow to bubbly ice from first principles," *Cryosphere*, vol. 16, no. 9, pp. 3861–3866, Sep. 2022, doi: 10.5194/tc-16-3861-2022.

[25] G. Picard et al., "The microwave snow grain size: A new concept to predict satellite observations over snow-covered regions," *AGU Adv.*, vol. 3, no. 4, Aug. 2022, Art. no. e2021AV000630, doi: 10.1029/2021av000630.

[26] G. Picard, M. Sandells, and H. Löwe, "SMRT: An active–passive microwave radiative transfer model for snow with multiple microstructure and scattering formulations (v1. 0)," *Geosci. Model Develop.*, vol. 11, no. 7, pp. 2763–2788, 2018, doi: 10.5194/gmd-11-2763-2018.

[27] A. Roy et al., "Brightness temperature simulations of the Canadian seasonal snowpack driven by measurements of the snow specific surface area," *IEEE Trans. Geosci. Remote Sens.*, vol. 51, no. 9, pp. 4692–4704, Sep. 2013, doi: 10.1109/TGRS.2012.2235842.

[28] A. Roy et al., "Microwave snow emission modeling uncertainties in boreal and subarctic environments," *Cryosphere*, vol. 10, no. 2, pp. 623–638, Mar. 2016, doi: 10.5194/tc-10-623-2016.

[29] A. Royer, F. Domine, A. Roy, A. Langlois, N. Marchand, and G. Davesne, "New northern snowpack classification linked to vegetation cover on a latitudinal mega-transect across northeastern Canada," *Écoscience*, vol. 28, nos. 3–4, pp. 225–242, Oct. 2021, doi: 10.1080/11956860.2021.1898775.

[30] A. Royer et al., "Comparison of commonly-used microwave radiative transfer models for snow remote sensing," *Remote Sens. Environ.*, vol. 190, pp. 247–259, Mar. 2017, doi: 10.1016/j.rse.2016.12.020.

[31] N. Rutter et al., "Effect of snow microstructure variability on Ku-band radar snow water equivalent retrievals," *Cryosphere*, vol. 13, no. 11, pp. 3045–3059, Nov. 2019, doi: 10.5194/tc-13-3045-2019.

[32] M. Sandells et al., "X-ray tomography-based microstructure representation in the snow microwave radiative transfer model," *IEEE Trans. Geosci. Remote Sens.*, vol. 60, 2022, Art. no. 4301115, doi: 10.1109/TGRS.2021.3086412.

[33] M. Sturm and C. Benson, "Scales of spatial heterogeneity for perennial and seasonal snow layers," *Ann. Glaciol.*, vol. 38, pp. 253–260, Jan. 2004, doi: 10.3189/172756404781815112.

[34] M. Tedesco, E. J. Kim, L. Li, and S. K. Lee, "Microwave remote sensing of snow: A review," *Remote Sens.*, vol. 12, no. 19, p. 3167, 2020.

[35] S. Torquato and J. Kim, "Nonlocal effective electromagnetic wave characteristics of composite media: Beyond the quasistatic regime," *Phys. Rev. X*, vol. 11, no. 2, Apr. 2021, Art. no. 021002, doi: 10.1103/physrevx.11.021002.

[36] C. Vargel et al., "Arctic and subarctic snow microstructure analysis for microwave brightness temperature simulations," *Remote Sens. Environ.*, vol. 242, Jun. 2020, Art. no. 111754, doi: 10.1016/j.rse.2020.

[37] V. Vionnet et al., "The detailed snowpack scheme crocus and its implementation in SURFEX v7.2," *Geoscientific Model Develop.*, vol. 5, no. 3, pp. 773–791, May 2012, doi: 10.5194/gmd-5-773-2012.

[38] L. Wang, J. Li, and J. Shi, "Progress in the remote sensing of snow parameters," *Adv. Atmos. Sci.*, vol. 36, no. 8, pp. 853–869, 2019.

[39] U. Wegmuller and C. Matzler, "Rough bare soil reflectivity model," *IEEE Trans. Geosci. Remote Sens.*, vol. 37, no. 3, pp. 1391–1395, May 1999, doi: 10.1109/36.763303.

[40] A. Wiesmann, C. Mätzler, and T. Weise, "Radiometric and structural measurements of snow samples," *Radio Sci.*, vol. 33, no. 2, pp. 273–289, Mar. 1998.

Alain Royer received the Ph.D. degree in geophysics from the University of Grenoble, Grenoble, France, in 1981.

From 1983 to 1988, he was a Natural Sciences and Engineering Research Council Fellow with the Centre d'Applications et de Recherches en Télédétection (CARTEL), Université de Sherbrooke, Sherbrooke, QC, Canada, where he has been a Professor, since 1988. From 2000 to 2010, he was also the Director of CARTEL. Retired in 2021, he continues his research works as an Associate Professor. His research interests include environmental geophysics, development of surface parameter retrieval algorithms from remote sensing data applied to northern climate change analysis.

Alexandre Roy (Member, IEEE) received the B.Sc. degree in physical geography from the Université de Montréal, Montreal, QC, Canada, in 2002, the M.Env. degree in remote sensing, and the Ph.D. degree in remote sensing from the Université de Sherbrooke, Sherbrooke, QC, Canada, in 2009 and 2013, respectively.

Since 2018, he is a Professor with the Département des Sciences de l'Environnement, Université du Québec à Trois-Rivières, Trois-Rivières, QC, Canada. He developed the Laboratoire de Recherche en Modélisation et Télédétection des Environnement Nordique (ReMoTE-Nord), which study the interactions between snow, soil, and vegetation and their impact on carbon fluxes in northern environments using remote sensing, modeling, and ground-based information.

Alexandre Langlois is a Professor with the University of Sherbrooke, Sherbrooke, QC, Canada. He is an expert in snow remote sensing and the geophysical processes that regulate its temporal, spatial, and vertical evolution. He has also worked on the close and complex interactions between the cryosphere and the changing climate. His remote sensing research focuses on microwaves at various scales and the development and validation of model simulation in the Arctic. He has also run a snow-monitoring program in Cambridge Bay, Victoria Island, NU, Canada, since 2013, and has developed a relationship with the Northern community.

Julien Meloche received the B.Sc. degree in physics from McGill University, Montreal, QC, Canada, in 2016, and the Ph.D. degree in physics of remote sensing from the University of Sherbrooke, Sherbrooke, QC, Canada, in 2022.

He was a Post-Doctoral Fellow at the University of Sherbrooke and was a Visiting Scholar at Northumbria University, Newcastle upon Tyne, U.K. He now works at the Climate Research Division, Environment and Climate Change Canada, Toronto, ON, Canada, as a Physical Scientist. His main research interests include microwave remote sensing of snow and radiative transfer modeling.

Ghislain Picard received the M.Sc. degree in remote sensing from the University of Paris VII, Paris, France, in 1997, and the Ph.D. degree from the Center d'Etudes Spatiale de la Biosphere (CESBIO), Toulouse, France, in 2002.

In 2005, he joined the Institut des Géosciences de l'Environnement, Université Grenoble-Alpes, Grenoble, France, where he has been a Full Professor, since 2018. He is involved in the development of innovative instruments for the characterization of the snow-physical properties and of optical and microwave radiative transfer (RT) models. His research interests include the Antarctic climate observed through the study of snow using a variety of remote sensing techniques and field experimentation.